Pergamon

0956-7151(93)E0055-8

Acta metall. mater. Vol. 42, No. 5, pp. 1509–1524, 1994

0956-7151/94 $6.00 + 0.00

THE IMPINGEMENT EFFECT OF AN INERT, IMMOBILE SECOND PHASE ON THE RECRYSTALLIZATION OF A MATRIX

C. F. PEZZEE and D. C. DUNAND

Department of Materials Science and Engineering, Massachusetts Institute of Technology, Cambridge, MA 02139, U.S.A.

(Received 29 April 1993; in revised form 11 November 1993)

Abstract—Two-dimensional computer simulations based on the cellular automaton algorithm were carried out to study the case of the recrystallization of a matrix containing inert, immobile particles. A range of particle area fractions, sizes and aspect ratios were investigated under continuous grain nucleation conditions, assuming that the effect of particles is limited to geometric impingement upon contact with the recrystallizing grains. Particles influence both overall recrystallization kinetics and the geometric characteristics of the recrystallized grain structure. Systematic deviations from the predictions by the Johnson, Mehl, Avrami, Kolmogorov (JMAK) theory for the recrystallization of a particle-free matrix are observed with increasing particle aspect ratio, and, to a lesser extent, particle fraction and size. These deviations are not predicted by a modified JMAK equation assuming that the impingement effect of inert particles is equivalent to that of non-growing grains, and result from the aspect ratio and size differences that exist between grains and particles. Inert particles also influence both mean size and mean aspect ratio of the recrystallized grains. While the normalized grain size distributions are unaffected by the particles, the normalized grain aspect ratio distributions exhibit significant variations as the particle geometric parameters are varied.

Résumé—On a entrepris des simulations par ordinateur basées sur l'algorithme de l'automate cellulaire à deux dimensions, afin d'étudier la recristallisation d'une matrice contenant des particules inertes et immobiles. Une gamme de fractions aréolaire, tailles et rapports d'allongement de particules est explorée avec des conditions de nucléation continue de grains, en supposant que le seul effet des particules est d'obstruer les grains lors de leur croissance par recristallisation. Les particules influencent aussi bien la cinétique de recristallisation que les caractéristiques géométriques de la structure des grains recristallisés. On observe des déviations systématiques des prédictions par Johnson, Mehl, Avrami et Kolmogorov (JMAK) pour la recristallisation d'une matrice sans particules; ces déviations augmentent avec une augmentation du rapport d'allongement des particules ainsi que, d'une moindre manière, avec une augmentation de la fraction et de la taille des particules. Ces déviations ne sont pas prédites par une équation de type JMAK modifiée, qui suppose que l'effet d'obstruction des particules est équivalent à celui de grains qui ne croissent pas, et sont le résultat de la différence de rapport d'allongement et de taille entre grains et particules. Les particules inertes influencent aussi la taille moyenne et le rapport d'allongement moyen des grains recristallisés. Alors que les distributions normalisées des tailles de grain ne sont pas influencées par les particules, les distributions normalisées des rapports d'allongement des grains changent de manière significative lorsque les paramètres géométriques des particules varient.

1. INTRODUCTION

The kinetics of crystallization and recrystallization by nucleation and growth of grains are described by the classical theory of Johnson and Mehl [1], Avrami [2, 3] and Kolmogorov [4] (JMAK). Analytical JMAK-type solutions are available only for simple cases such as continuous nucleation, site-saturated nucleation and continuously varying nucleation rates [5]. More complex conditions (e.g. space- or time-dependent nucleation or growth rates for cases such as dynamic recrystallization, deformation bands or multiple phases) can be untractable analytically, leading many investigators to use computer simulation techniques to investigate crystallization and recrystallization kinetics and the topological characteristics of the grains. Algorithms used for these simulations are based on (i) the equation of motion of grain boundaries [6–10], (ii) binary tree construction on a grid [11–15], (iii) the Monte-Carlo method [16–20] and (iv) cellular automata [21–23]. The last three methods discretize space in two- or three-dimensional cells.

As reviewed recently by Rollett *et al.* [24], the presence of an inert second phase in a matrix undergoing recrystallization can strongly influence the kinetics of the process (i) by increasing the rate of nucleation at the matrix–particle interface which is locally more deformed, and/or (ii) by inhibiting by Zener pinning the coarsening of subgrains that are

responsible for the nucleation of the recrystallized grains, thus decreasing the recrystallization nucleation rate. Rollett *et al.* [19, 24] have studied by two-dimensional Monte Carlo simulations the recrystallization kinetics of a matrix containing equiaxed particles with a size equal to that of the cells, i.e. much smaller than the final grain size. They concluded that at high stored energies, the recrystallization growth is not affected by the particles. At low stored energies, however, particle pinning of both nuclei and larger grains was found to occur, thus inhibiting recrystallization. The nucleation stage was also affected by the particles, which acted as heterogeneous nucleation sites. Grain coarsening during and after recrystallization was found to be strongly inhibited by particles, which thus further affected the grain microstructure.

While, as shown above, Zener drag on recrystallizing grains by well-dispersed, small particles can be neglected when the driving force for recrystallization is high, that effect can become important when the particles are spatially clustered, their shape is not equiaxed or their volume fraction is high. Saetre *et al.* [14] and Nes *et al.* [25] investigated the recrystallization behavior of a matrix containing stringers of densely spaced particles, typically found in rolled metals where particles are clustered in sheets parallel to the rolling direction. They analytically derived the grain boundary velocity as a function of the particle shape and boundary orientation with respect to the rolling direction. Computer simulations using these values generated pancake-shaped grains displaying a morphology and distribution form in good agreement with experimental data from rolled Al–Mn alloys. Furu *et al.* [5, 15, 26] investigated both analytically and by computer simulation the effect of inhomogenously distributed, particle-stimulated nucleation sites. Two cases were examined: (i) nucleation of a single grain by each particle, and (ii) site saturation at the surface of the particles. The former case was in better agreement than the latter with experimental results on recrystallized aluminum alloys. Humphreys [9, 27] recently explored the effect of a dispersion of small equiaxed particles on the nucleation and growth of recrystallized grains, using a network model where subgrains as well as grains were considered. The model operates on a smaller scale than those reviewed above and addresses the early stages of recrystallization for materials such as aluminum, where subgrains play a large role in that process. For nucleation, a gradient of subgrain energies near the particles was introduced and the particle–matrix interface was modeled as a high-angle grain boundary. To take into account the effect of particles on growth, a pinning force assigned to the particles was added to the forces due to grain boundary energies.

The effects reported above, which particles exert on the nucleation and growth of recrystallizing grains, are *thermodynamical* in nature, i.e. they can be described by considering the energy of the system. Inert particles also have a purely *geometric* effect resulting from the impingement they exert on grains: the growth of a recrystallizing grain is stopped at the points where it contacts a particle. This interaction may become important when the specific area of matrix–particle interface is high, i.e. for high volume fractions, high aspect ratios and small sizes of particles, in such materials as those formed by phase separation through solidification or precipitation in the solid state, in metal- or ceramic matrix composites and in foamed materials (where the second phase is formed by pores). The purpose of the present study is to explore the geometric impingement effect of an inert, immobile second phase on the recrystallization kinetics of a matrix as well as the resulting grain topology. Parameters being varied are particle size, area fraction and aspect ratio.

2. COMPUTATIONAL PROCEDURES

As described in more details by Hesselbarth and Göbel [21], a cellular automaton for recrystallization consists of a field of cells with two possible states—recrystallized and unrecrystallized—which evolves with time according to local topological rules. Time is discretized in time-steps which are further divided in two sequential events: growth and nucleation. In the nucleation phase, nuclei consisting of a single recrystallized cell are distributed randomly in the field; only those that are nucleated on an unrecrystallized cell are considered. For a constant nucleation rate by unit area, the total number of new nuclei added to the field for each time step thus decreases with time as a result of the shrinking unrecrystallized space available for nucleation. In the growth phase, the entire field is updated according to the following deterministic rules:

(1) a recrystallized cell remains recrystallized;
(2) an unrecrystallized cell becomes recrystallized if at least one of its neighbors is recrystallized. It becomes part of the same grain as the recrystallized neighbor.

The following rules were added to the original model by Hesselbarth and Göbel [21] to take into account the presence of inert particles:

(3) at time $t = 0$, second-phase particles are placed randomly on the field with a minimum spacing of two cells between particles; these particles cannot grow.
(4) matrix grains neither nucleate nor grow within particles.

The following parameters were used in the present study:

(i) a two-dimensional field of 262,144 (512^2) square cells oriented along orthogonal axes with periodic boundary conditions;
(ii) homogenous nucleation conditions, with a nucleation rate of $4 \cdot 10^{-4}$ for each time step;

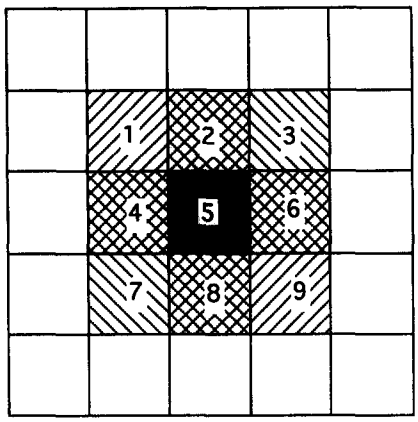

Fig. 1. Alternating six-cell neighborhood around cell 5: (1, 2, 4, 6, 8, 9) followed by (2, 3, 4, 6, 7, 8).

(iii) a neighborhood of six alternating neighbors for the growth phase (Fig. 1), resulting in equiaxed octagonal grains before impingement. Other possible neighborhoods can be defined, resulting in different growth rates but giving the same Avrami exponent for particle-free recrystallization [21]. The above neighborhood yields recrystallized structures with the largest number of grain boundary orientations [22], and thus gives structures closest to those observed in recrystallized materials. Since no nuclei exist at time $t = 0$, growth does not take place in the first time step $t = 1$ which consists of a nucleation event only.

(iv) an unrecrystallized cell with recrystallized neighbors belonging to more than one grain becomes part of any of the competing grains with the same probability.

Three parameters related to the geometry of the second phase were varied: particle size a (measured in number of cells), particle area fraction f and particle aspect ratio r. A set of baseline values ($a = 64$, $f = 0.125$ and $r = 4$) was chosen, and each parameter was varied separately according to Table 1, keeping the other two parameters fixed at their baseline values. After each time step, the area fraction of recrystallized matrix x was calculated as the ratio of recrystallized matrix area to total matrix area. The grain size A (measured in number of cells) and grain aspect ratio R—defined as the ratio (larger than 1) of the projections of the grain along the two orthogonal axes—were calculated for each grain at the end of the simulation. The resulting distributions for A and R were analyzed using non-parametric statistics (Appendix 1). All statistical results were determined using two simulations carried out with the same parameters but different random spatial distributions of particle and nuclei.

Table 1. Particle geometric characteristics varied in the parametric studies (baseline values are in bold characters)

Size a [cells]	4	16	**64**	256	
Area fraction f [−]	0	0.03125	0.0625	**0.125**	0.25
Aspect ratio r [−]	1	**4**	16	64	

3. RESULTS

Figure 2(a) and (b) illustrates the impinging effect upon a single recrystallizing grain of particles with different aspect ratios but same total area. The contours correspond to the location of the grain boundary at different time-steps. A grain nucleating between regions of high area fraction of small, equiaxed particles [Fig. 2(a)] grows through these regions virtually unimpeded by the particles which are rapidly engulfed. Except for two small ledges, the grain has the octagonal shape expected for a grain growing in a particle-free matrix. However, if the small, equiaxed particles of Fig. 2(a) are replaced by elongated particles [two-dimensional "fibers", Fig. 2(b)] with the same total area, the growth of the grain is markedly modified. Five distinct stages are observed: (1) unimpeded, two-dimensional growth before contact with the fibers ($t \leqslant 7$); (2) channeled,

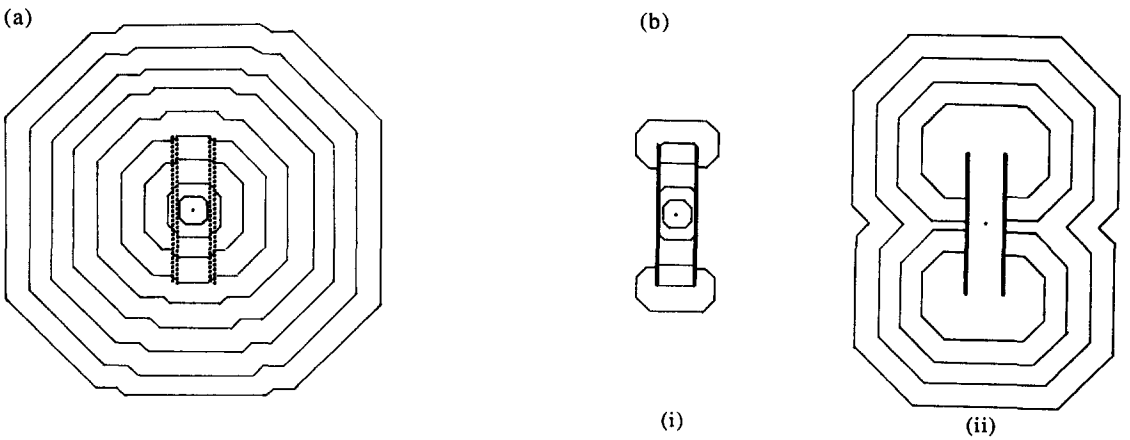

Fig. 2. Different stages of growth of a single grain in a matrix containing the same area fraction of particles of different shapes and aspect ratio: (a) 128 small, equiaxed particles for times $t = 1$, 6, 11, 21, 31, 41, 51, 61, 71, 81; (b) 2 large, elongated fibers: (i) for times $t = 1$, 6, 11, 21, 31, 41; (ii) for times $t = 51$, 61, 71, 81.

one-dimensional growth between the fibers, with the mobile grain boundaries perpendicular to the fibers ($7 < t \leqslant 31$); (3) two-dimensional growth from the recrystallized regions at both ends of the channel formed by the fibers ($31 < t \leqslant 63$); (4) merging of these two distinct regions, with the formation of a groove on the grain boundary parallel to the fibers ($63 < t \leqslant 90$); (5) disappearance of the groove and further unimpeded growth of the grain ($t > 90$). The resulting grain [Fig. 2(bii)] shows a flattened octagonal shape, the height of which corresponds to the height of the regular octagonal shape of the freely growing grain [Fig. 2(a)].

Figure 3(a–b) shows the time evolution of the topological parameters (aspect ratio R and square root of the area $A^{1/2}$) for the grains in Fig. 2(a, b). As expected for the case of a freely growing grain, the grain growing through the array of small, equiaxed particles [Fig. 2(a)] shows a constant aspect ratio $R = 1$ and an area A increasing with the square of time. On the other hand, the aspect ratio of the grain growing between the two fibers increases from unity at the end of stage (1) to a maximum value at the end of stage (2), and decreases monotonously after growth becomes two-dimensional again (stages 3–5). The five stages described above are also clearly visible in Fig. 3(b) for the area of the grain growing between the fibers: from a normal two-dimensional rate [stage (1)], the rate of growth goes through a minimum when the grain is channeled by the fibers [stage (2)], followed by a maximum when the two end regions of the grain are growing independently in two-dimensional manner [stage (3)] until it matches again the rate of a freely growing grain [stage (5)].

In Figs 4–6, the whole field of the cellular automaton is reproduced at different times in the simulation. The particles are filled, the grain boundaries are shown as lines and the origin of each grain, corresponding to the position of its nucleus, is marked as a filled cell within each grain. The computational procedure (iv) described above results in ragged grain-boundaries, as also observed in Monte-Carlo recrystallization simulations by Srolovitz *et al.* [16]. Figure 4(a–c), corresponding to the matrix without particle explored by Hesselbarth and Göbel [21], shows the classical stages of growth with minimal impingement [Fig. 4(a)], growth with limited impingement due to neighboring grains [Fig. 4(b)], and complete impingement resulting in a fully recrystallized field [Fig. 4(c)]. Figure 5(a–c) depicts the case of a matrix containing particles with baseline parameters (size $a = 64$ cells, area fraction $f = 0.125$ and aspect ratio $r = 4$). It is apparent that impingement between particles and grains occurs early for grains which nucleated near particles [Fig. 5(a)]. With about 50% of the structure recrystallized, most grains which have grown for more than three time-steps are in contact with both particles and other grains [Fig. 5(b)]. In the final structure [Fig. 5(c)] the majority of the grains contacts one particle, with most of the

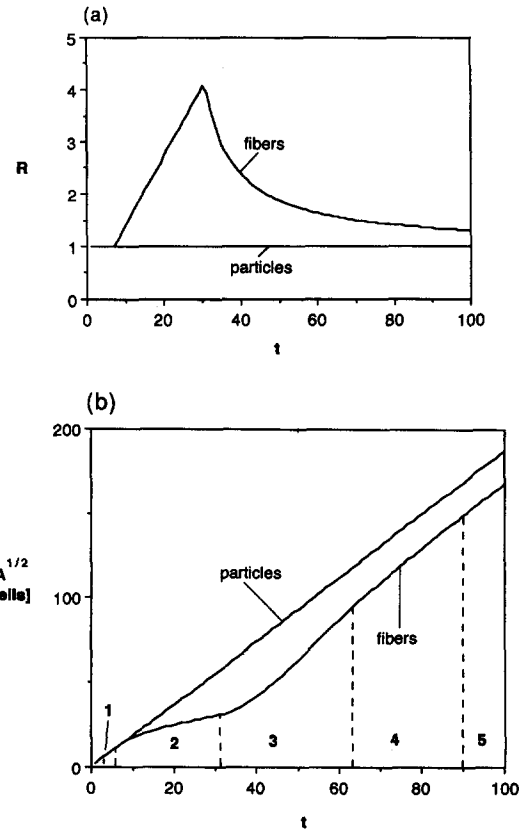

Fig. 3. (a) Grain aspect ratio R as a function of time for the cases depicted in Fig. 2(a, b). (b) Square root of grain size $A^{1/2}$ as a function of time for the cases depicted in Fig. 2(a, b). Numbered regions ae described in the text.

other grains in contact with zero or two particles. Figure 6(a–c) corresponds to the evolution of recrystallization of a matrix containing particles with the highest aspect ratio explored ($r = 64$). Most grains are in contact with at least one two-dimensional fiber early in their growth [Fig. 6(a)]. As grain growth becomes channeled between fibers [Fig. 6(b)], the final grain structure is markedly elongated in the direction of the fibers, with about 75% of the grain population in contact with at least two fibers [Fig. 6(c)]. In the final structure, most boundaries between grains are perpendicular to the fibers, and few boundaries between grains exist parallel to the fibers, as the average length of the grains in that direction is smaller than the fiber length.

In Fig. 7(a–c), the area fraction of recrystallized matrix x is plotted as a function of time t for some of the particle parameters explored. The curves have a sigmoidal shape, typical of a JMAK-type equation:

$$x = 1 - \exp(-kt^n), \qquad (1)$$

where k is a function of the nucleation and growth rates and n is the Avrami exponent (Appendix 2). It is apparent that recrystallization is slowed as the particle perimeter per unit area matrix is increased, i.e. with increasing particle area fraction and aspect ratio and with decreasing particle size. The same data

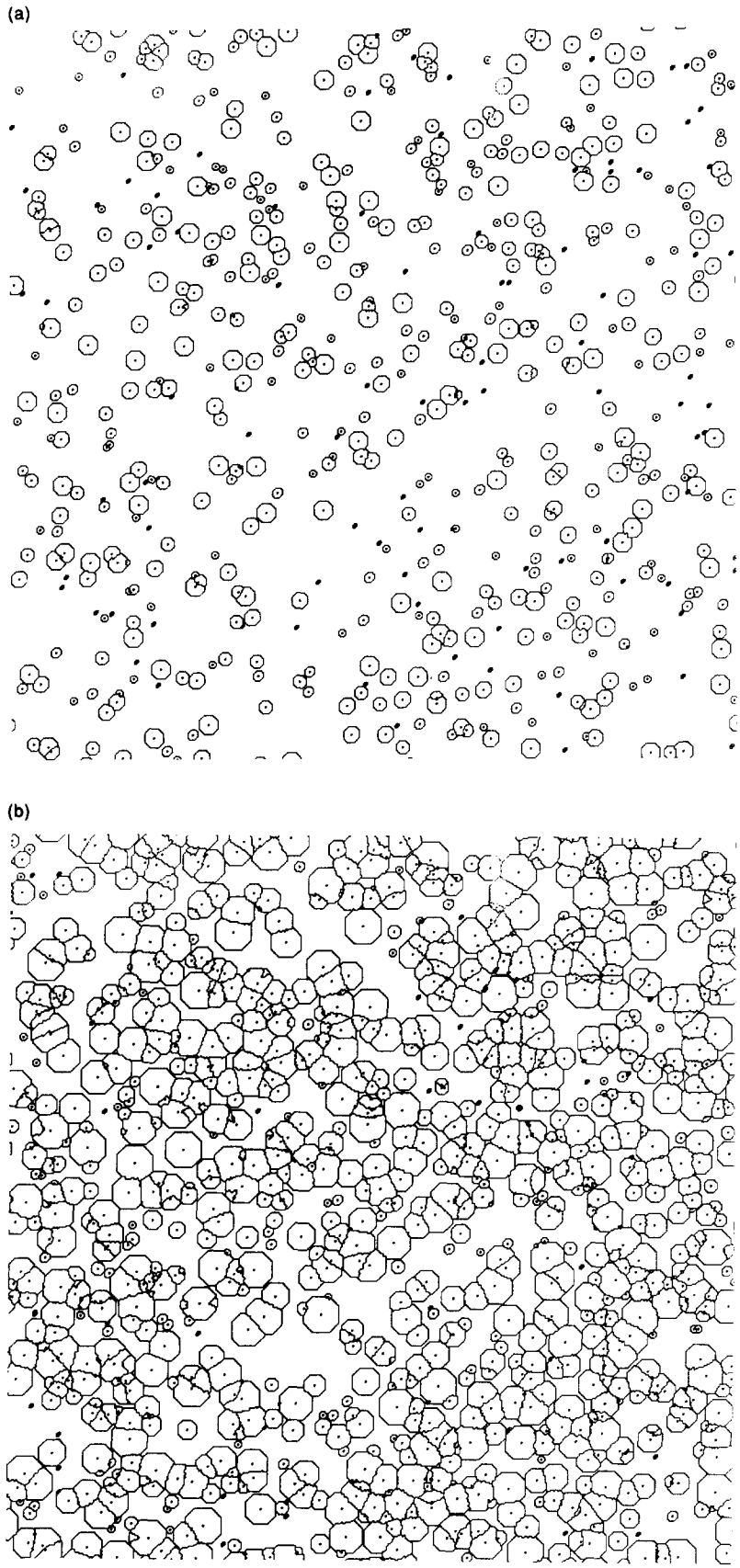

Fig. 4(a, b). *Caption overleaf.*

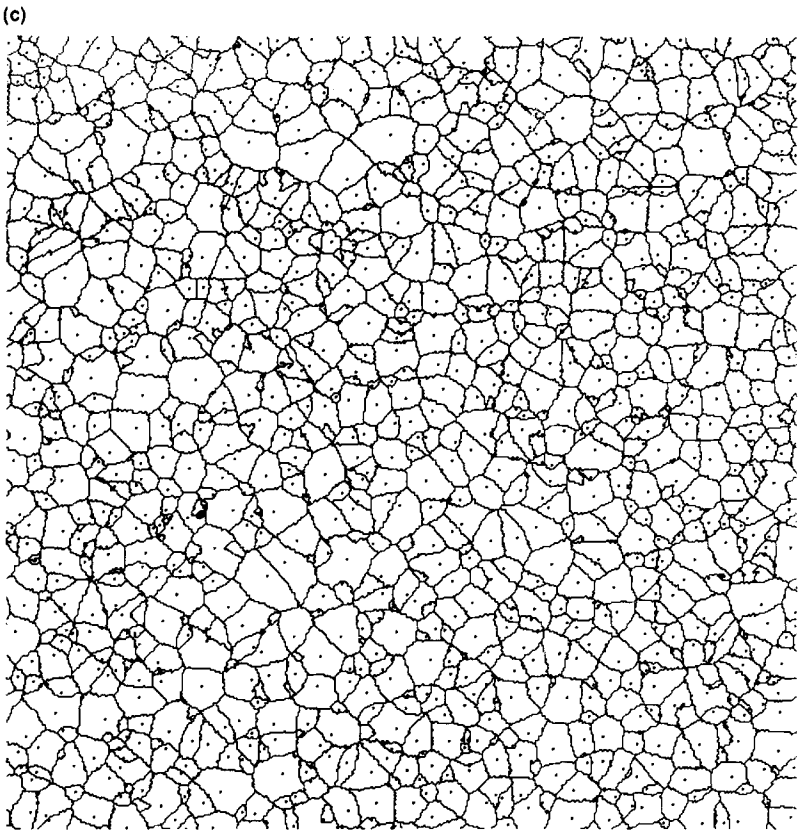

Fig. 4. Recrystallized field without particles at different times: (a) early stage, (b) intermediate stage, (c) complete recrystallization.

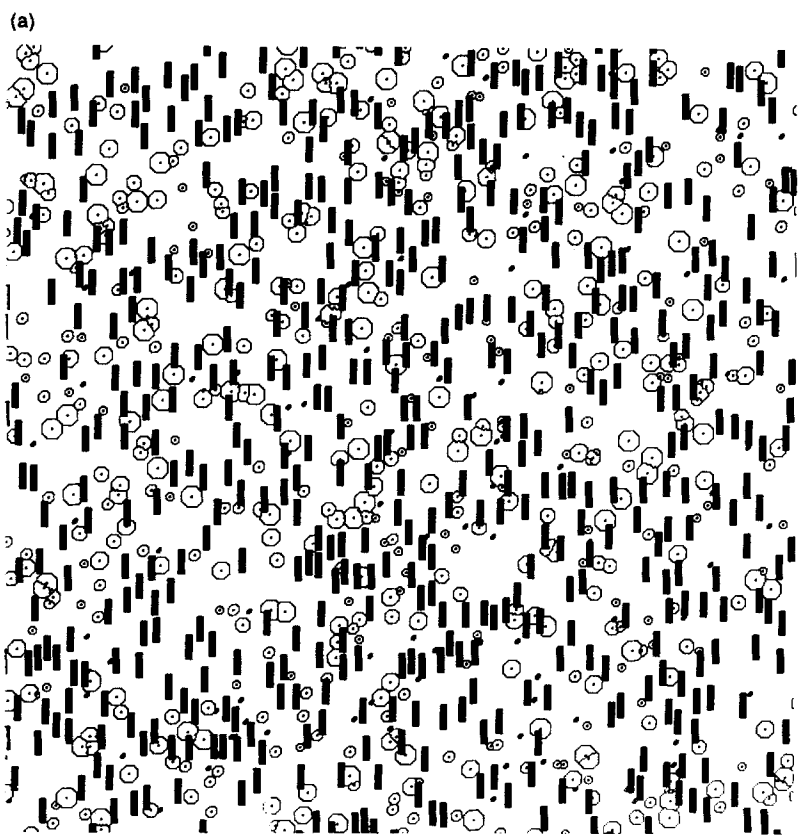

Fig. 5(a). *Caption on facing page.*

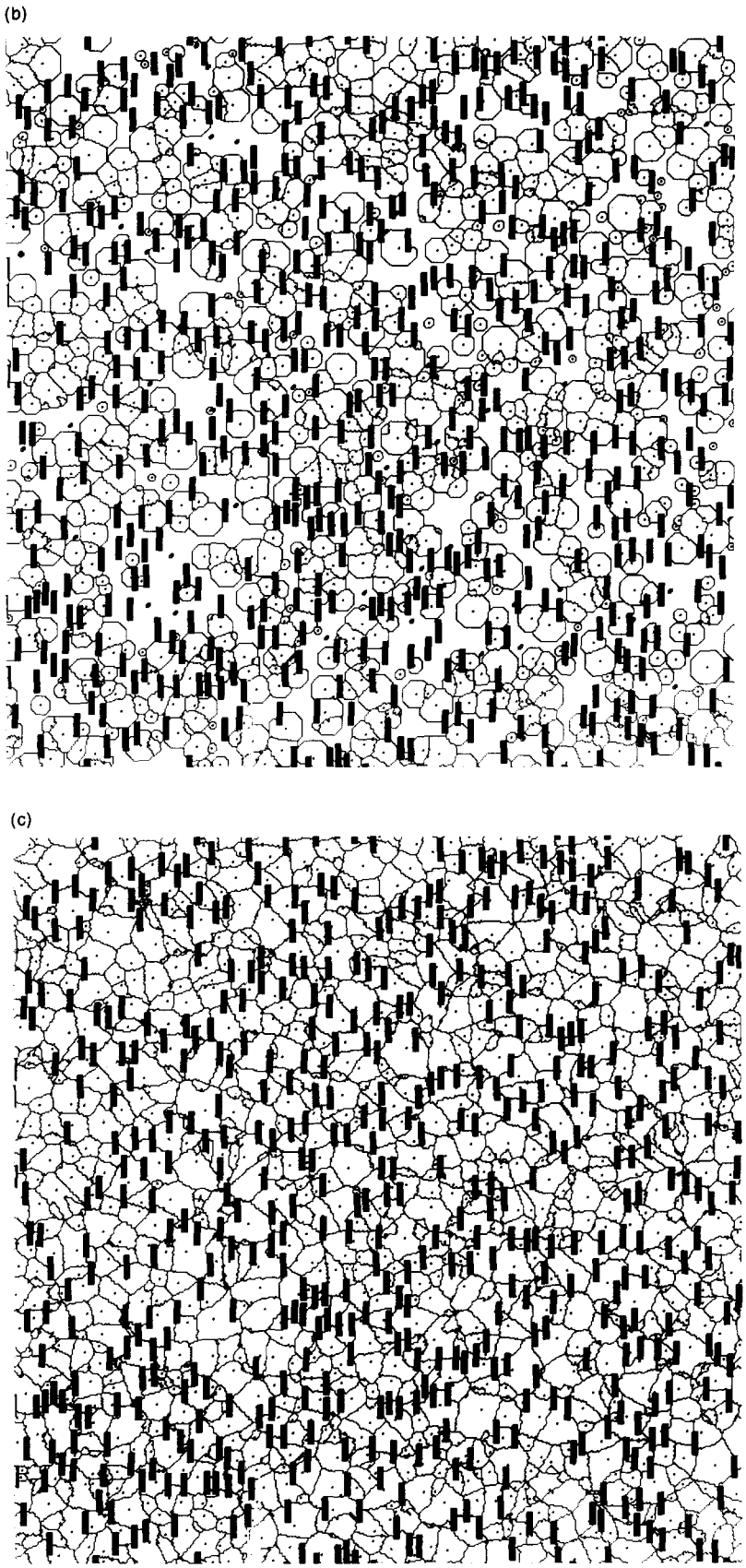

Fig. 5. Recrystallized field containing particles with the baseline parameters $a = 64$ cells, $f = 0.125$ and $r = 4$ at different times: (a) early stage, (b) intermediate stage, (c) complete recrystallization.

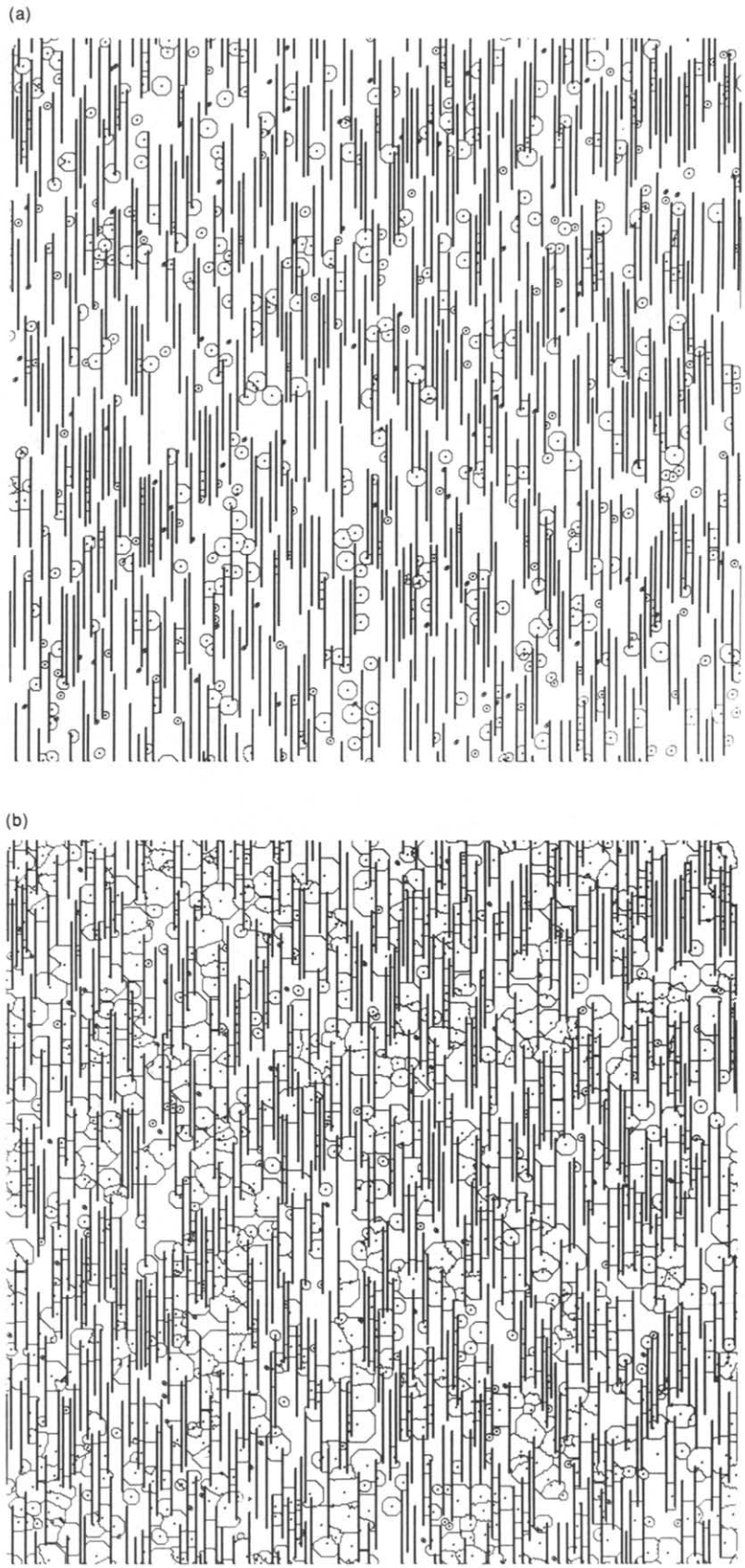

Fig. 6(a, b). *Caption on facing page.*

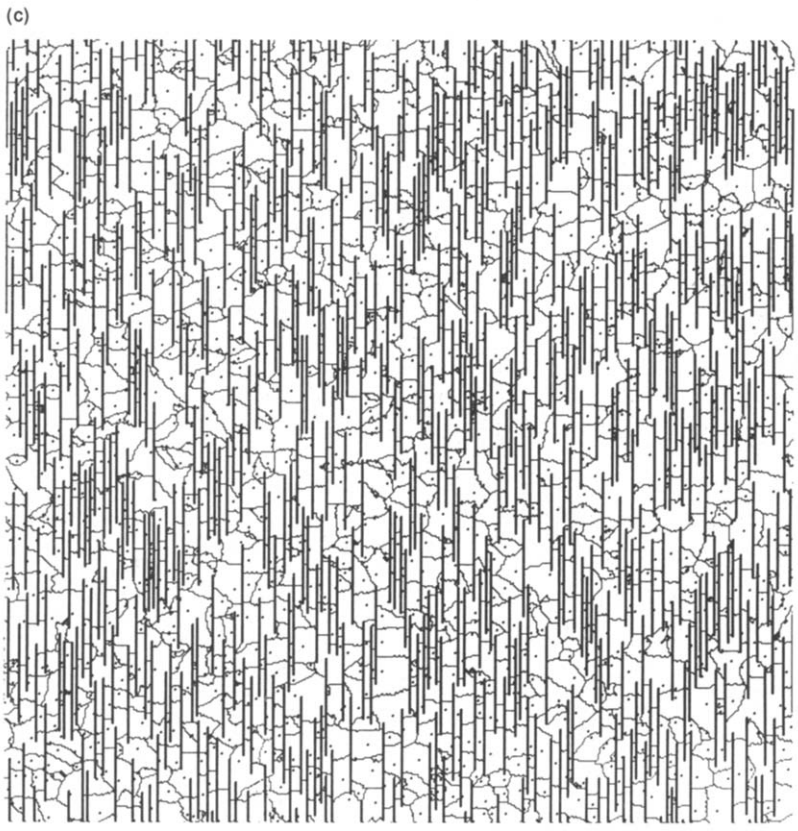

Fig. 6. Recrystallized field containing particles with parameters $a = 64$ cells, $f = 0.125$ and $r = 64$ at different times: (a) early stage, (b) intermediate stage, (c) complete recrystallization.

are shown in Fig. 8(a–c) in double logarithmic plots, the slopes of which correspond to the Avrami exponent n, which is also given as a function of time in these figures. As expected, the theoretical value $n = 3$ is found for the case where the field does not contain any particle [Fig. 8(b), $f = 0$], but significant departures from the expected value are observed for some of the particle parameters explored.

Since, as shown in Fig. 7(a–c), an increasing particle specific perimeter increases the time necessary for full recrystallization, the total number of grains nucleated during the recrystallization period is also expected to increase, and thus the mean grain size $\bar{A}$ after complete recrystallization is expected to decrease. This is indeed the case, as seen in Fig. 9(a–c), which shows $\bar{A}$, normalized by the mean grain size of the base line case $\bar{A}_0$ for all explored particle parameters. Also displayed in Fig. 9(a–c) is the normalized mean aspect ratio of recrystallized grains $\bar{R}/\bar{R}_0$, which increases with increasing values of a, f, and r. The normalized grain size distribution $A/\bar{A}$ and aspect ratio distribution $R/\bar{R}$ are given in Figs 10(a–c) and 11(a–c) for some of the particle parameters explored.

4. DISCUSSION

In this study, it was assumed that the second phase particles have no effect, other than the geometric impingement they exert on growing grains. This assumption allows to study separately the impingement effect, which is usually found superimposed with other effects in experimental studies of recrystallization in two-phase materials: particles can stimulate the nucleation stage by increasing the amount of heterogeneous nucleation sites, retard the growth kinetics by pinning grain boundaries, or be pushed by the moving boundaries [20].

4.1. Kinetics of recrystallization

As shown in Appendix 2, the results of the original JMAK derivation [equation (1)] are unchanged if inert, discontinuous particles are introduced in the matrix, because the particle volume can be subtracted from the total volume. The important assumption underlying this result is that overall impingement by the particles is isotropic and proportional to their volume fraction. Special cases of anisotropic impingement can however be treated within the JMAK framework: in the three-dimensional case, full impingement in one or two directions is modeled by assigning a zero growth rate in these directions, leading to two- or one-dimensional growth with Avrami exponent of $n = 3$ and $n = 2$ respectively for continuous nucleation conditions [3]. Similarly, in two-dimensional recrystallization, complete lack of growth in one or two directions leads to an Avrami

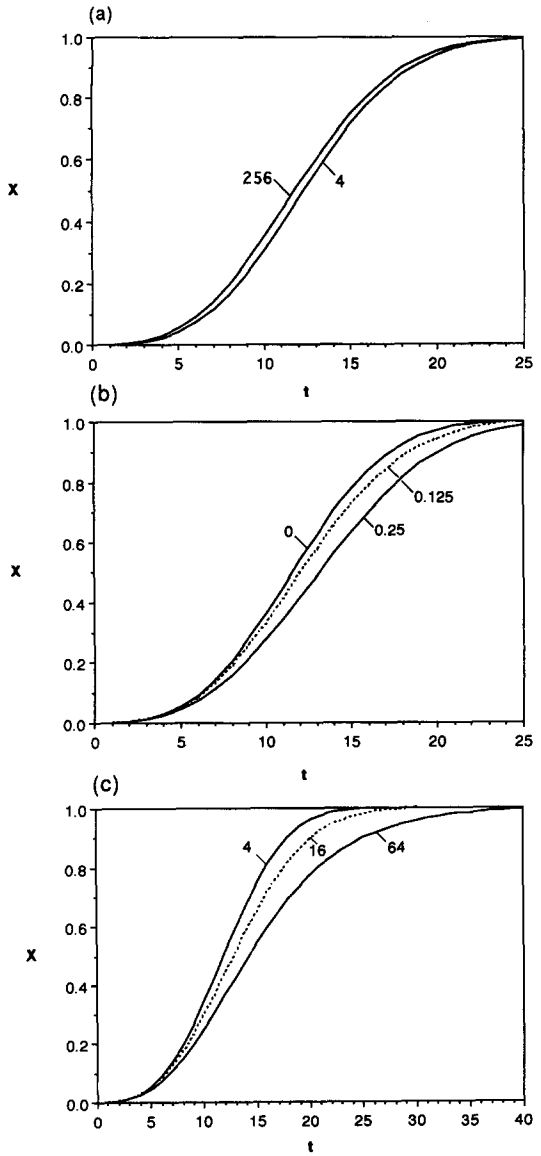

Fig. 7. Matrix fraction recrystallized x as a function of time t for a matrix containing particles with varying (a) size a, (b) area fraction f, (c) aspect ratio r.

exponent of $n = 2$ and $n = 1$ respectively. Total impingement in one direction corresponds for instance to the case of a matrix containing elongated particles with a length larger than the length of the field, preventing all growth in the direction perpendicular to the fiber axis [Fig. 2(bi)]. Therefore, impingement by a discontinuous second phase is expected to become of importance when at least one of the particle's dimensions becomes comparable to the final grain size, and when the particle volume fraction is large enough that a significant number of grains interact with particles. However, unlike the cases described above where full impingement in one or more direction exists, partial impingement resulting from a discontinuous second phase cannot be modelled simply by modifying the overall growth rates in the JMAK derivation.

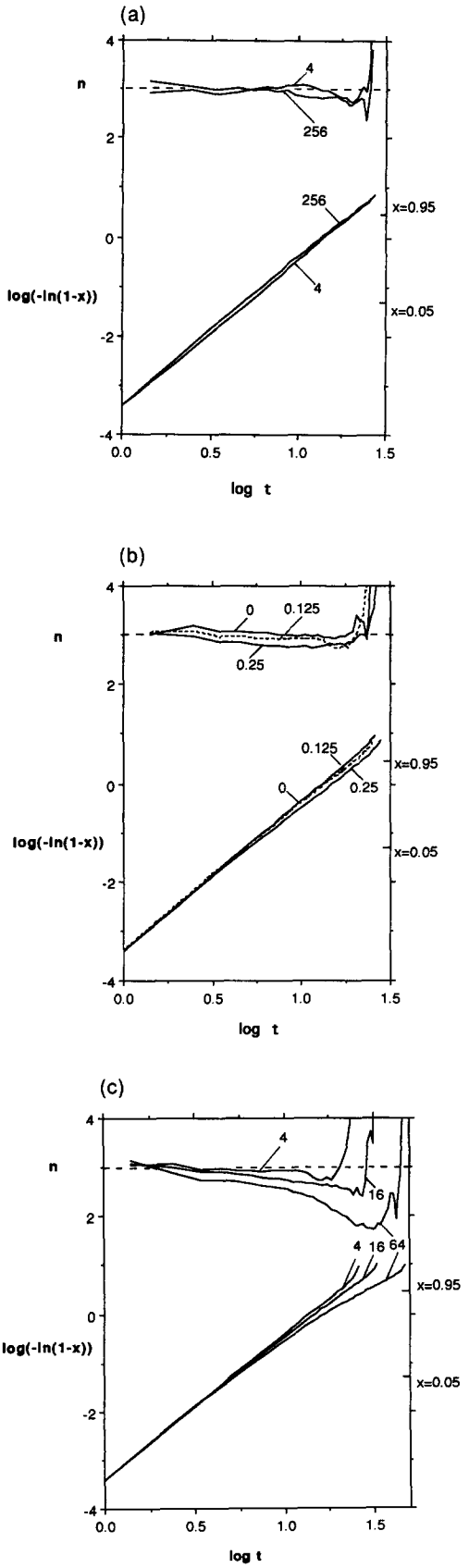

Fig. 8. JMAK plots with the time evolution of the Avrami exponent n for the same particle parameters as in Fig. 7. (a) Size a, (b) area fraction f, (c) aspect ratio r.

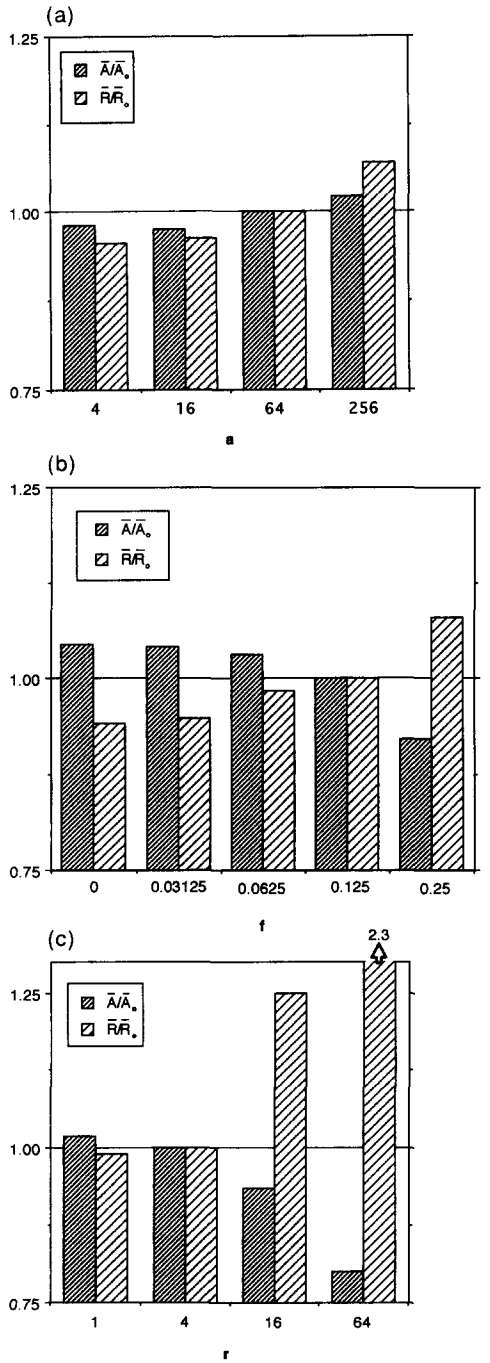

Fig. 9. Histograms of mean grain area $\bar{A}$ (normalized by the mean grain area of the baseline condition $\bar{A}_0$) and mean grain aspect ratio $\bar{R}$ (normalized by the mean grain aspect ratio of the baseline condition $\bar{R}_0$) for a fully recrystallized matrix containing particles with varying (a) size a, (b) area fraction f, (c) aspect ratio r.

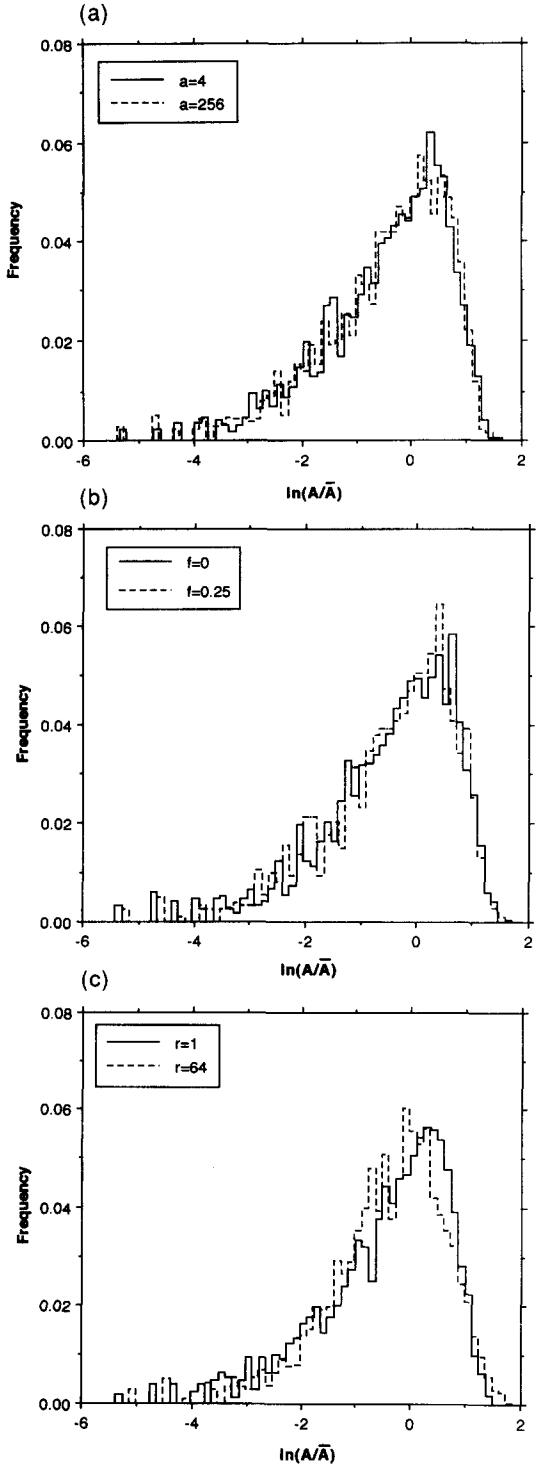

Fig. 10. Distribution of normalized grain size $A/\bar{A}$ for a fully recrystallized matrix containing particles with varying (a) size a, (b) area fraction f, (c) aspect ratio r.

At the local scale of the cell or grain boundary, impingement between two grains, on the one hand, and between a grain and a particle, on the other, has a similar effect: growth is locally stopped. At the larger scale of grains, however, the two types of impingements are different because (i) particles, unlike grains, do not grow with time and (ii) particles may be non-equiaxed. Dissimilarity (i) results in an overall grain-particle impingement which increases first with time, as an increasing number of grains contact particles, and may then decrease, as particles are engulfed by grains. On the other hand, the overall grain-grain impingement does not decrease with time, since all grains are growing simultaneously. However,

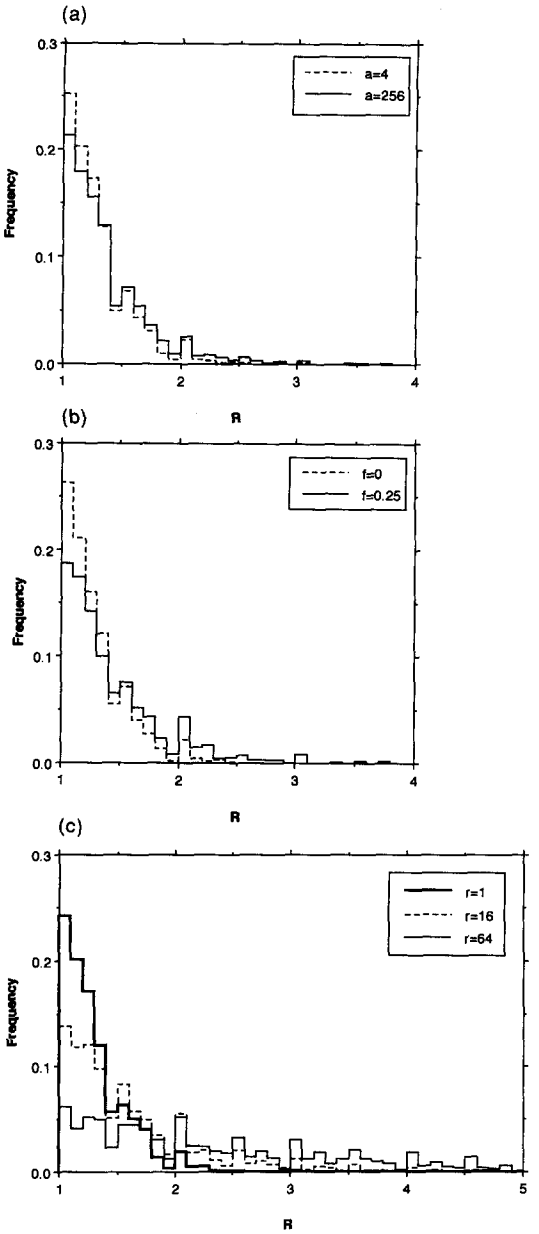

Fig. 11. Distribution of grain aspect ratio R for a fully recrystallized matrix containing particles with varying (a) size a, (b) area fraction f, (c) aspect ratio r.

as shown in Appendix 2, the presence of an inert second phase does not affect the overall kinetics of the matrix, provided overall impingement by the particles is isotropic and proportional to their volume fraction [equation (A4)]. Dissimilarity (ii)—the shape difference that exists between grains and non-equiaxed particles—may lead to a situation that violates the above assumption. The impingement between a grain and an elongated particle is maximum (minimum, respectively) when the grain boundary moves in a direction orthogonal (parallel, respectively) to the particle main axis. Elongated particles exert an impingement which is total in the direction perpendicular to their long axis, as long as the grain does not engulf the particle [Figs 2(b) and 3]. As a result, significant deviation from the JMAK equation can occur, and the topology of the recrystallized grains can be altered by the presence of the particles, as shown below. On the other hand, small particles are rapidly engulfed, with no effect on overall growth kinetics [Figs 2(a) and 3], as shown analytically in Appendix 2 and as found in Monte-Carlo simulations by Rollett *et al.* [19, 24]

The Avrami exponent shown in Fig. 8(b) for a particle-free matrix ($f = 0$) is close to the value of $n = 3$ for matrix recrystallized fractions between $x = 0.05$ and $x = 0.95$, as expected from equation (1) and as also found by Hesselbarth and Göbel [21] in cellular automaton simulations carried under the same nucleation and growth conditions. These authors ascribed the deviations at low and high recrystallized fractions (also visible in Fig. 8) to stochastic variations resulting from the small number of grains growing. As the particle area fraction f increases, the Avrami exponent plotted in Fig. 8(b) decreases, as expected from an increasing impingement between particles and grains. An increasing particle size a, at constant particle area fraction and aspect ratio, yields Avrami exponents below $n = 3$ and decreasing with time up to $x = 0.95$ [Fig. 8(a)]. The overall effect is however small and the JMAK curves are virtually superimposed.

The most important deviations from the unimpeded case are found when the particle aspect ratio r is increased [Fig. 8(c)]. While for $r = 4$, the Avrami exponent is close to $n = 3$ until values of about $x = 0.65$, for $r = 16$, the Avrami exponent decreases rapidly from $n = 3$ to values as low as $n = 2.4$ as recrystallization proceeds. This can be explained by the anisotropic impingement effect discussed above and illustrated in Figs 2(b), 3 and 6, whereby growth under continuous nucleation conditions occurs in a regime intermediate between two-dimensional growth ($n = 3$) and one-dimensional growth ($n = 2$). The effect is even stronger for a particle aspect ratio $r = 64$, where the Avrami exponent decreases steadily from $n = 3$ at low recrystallized area fractions to $n = 1.7$ for $x = 0.95$. A value below $n = 2$ corresponds to a case between continuous nucleation without growth ($n = 1$) and continuous nucleation with unidirectional growth ($n = 2$). Oriented elongated particles have thus a strong effect on the kinetics of recrystallization, as a result of anisotropic impingement between grains and particles.

4.2. *Grain topology*

We now consider the effect of particle impingement on the geometrical characteristics of the recrystallized grains. The grain mean area $\bar{A}$ departs from the baseline grain mean area $\bar{A}_0$ as the particle size, area fraction and aspect ratio vary [Fig. 9(a–c)]. The observed variation (between 1.9 and 20.5%) is large compared to the difference of 0.4% found between two simulations carried out under baseline conditions

($\bar{A} = 214.1$ and $\bar{A} = 215.3$). In all cases, $\bar{A}$ decreases as the particle perimeter per unit area matrix increases, i.e. with decreasing particle size and increasing particle aspect ratio and area fraction. The effect of particle size is however much smaller than that of the two other parameters, in accord with the observation by Rollett *et al.* [19, 24] that very small particles have little influence on simulated recrystallization kinetics. Furthermore, the mean grain aspect ratio $\bar{R}$ increases with increasing particle aspect ratio, size and area fraction [Fig. 9(a–c)]. As for the grain mean area, the differences in mean grain aspect ratios between two baseline runs is much smaller than that observed when one of the particle parameters is varied.

It is difficult to evaluate by visual inspection of Figs 10 and 11 how significant the difference between distributions is, as particle parameters are varied. The normal deviate Z (defined in Appendix 1) is used as a quantitative measure of the difference between the baseline distribution and the distributions from the parametric study. To take into account the shift of distribution due to differences in mean value, we list in Table 2 the deviate Z_R for the distribution of grain aspect ratio normalized by their mean grain aspect ratio $R/\bar{R}$, and the deviate Z_A for the normalized grain size distribution $A/\bar{A}$. For comparison, Z_R and Z_A were first determined for two simulations performed under the same baseline particle parameter conditions, yielding values of $Z_R = 1.11$ and $Z_A = 0.0533$. The non-zero values of Z are due to the different locations of particles and nuclei for the two baseline simulations. These normal deviates are however smaller than the critical normal deviate value of $Z_c = 1.96$ for a 5% significance level (corresponding to the threshold below which 95% of the Z values from two identical populations is expected to be). Normal deviates between the baseline condition and the other conditions explored (Table 2) show that, for most particle sizes, area fractions and aspect ratios, values of Z_R are above the threshold Z_c for a significance level of 5% (with the exception of $r = 1$ and $f = 0.0625$). The numerical value of Z_R increases as the difference between the particle parameters increases, indicating that the normalized distributions become more different. In contrast to the strong effect found for the normalized grain aspect ratio distributions, all Z_A values listed in Table 2, calculated for the distributions of normalized grain sizes, fall significantly below the threshold of $Z_c = 1.96$ for a 5% significance level. It can thus be concluded that, while the mean grain size varies significantly when varying the particle parameters [Fig. 9], the grain size distributions can be scaled to the baseline condition. Normalization does not however compensate for the differences found in the grain aspect ratio distribution.

All distributions of grain aspect ratios (Fig. 11) exhibit systematic peaks and troughs at grain aspect ratios values corresponding to ratios of small integers x/y: peaks are found for $R = 1/1$, $3/2$, $2/1$, etc. and troughs for $R = 5/7$, $10/9$, etc. If the frequency of all possible combinations x/y is plotted, where x and y are positive integers less than a maximum value x_{max}, the same characteristic peaks and troughs are found for small values of x_{max} [Fig. 12(a)]. This noise however decreases in importance as x_{max} increases. The same phenomenon is true for the distribution of all possible products $x \cdot y$ [Fig. 12(b)], which mimics the noise found in the distribution of grain area (Fig. 10). The lack of smoothness of the distributions of grain sizes and aspect ratios (Figs 10 and 11) is thus the result of the finite length of the cells used in the simulation and the bins used for the distribution: as the size of the cell decreases compared to the size of the grain, this effect is expected to become less important. We note that this artifact is not peculiar to cellular automata models, but is shared by all other computer studies where space is discretized.

The recrystallized grain sizes (Fig. 10) show a significantly more sharply peaked distribution around the mean value than the random distribution [Fig. 12(b)] which exhibits a longer tail for small abcissa values. This is not unexpected, as the grains resulting from the recrystallization process are the result of mutual interactions during impingement, leading to a distribution of shapes which is plane-filling and thus non-random. We note that grain growth by coarsening during or after recrystallization, which cannot be simulated with the algorithm used in this study, further skews these distributions towards larger grain size, as found in many computer simulations of grain growth for matrices with or without particles [28–34].

The distribution of aspect ratios for $f = 0$ [Fig. 11(b)] also exhibits a much higher peak than the random distribution [Fig. 12(a)]. Thus, as expected from the condition that impingement is isotropic upon recrystallization without particles, equiaxed or nearly-equiaxed grains are much more frequent than in a random distribution. However, as the particle size, aspect ratio and area fraction increase, the grain aspect ratio distribution broadens. The effect is strongest with particles with high aspect ratios r which induce strong anisotropic impingement [Fig. 2(b)]: for $r = 64$ [Fig. 11(c)], the simulated grain aspect ratio distribution is flatter and broader than the random distribution [Fig. 12(a)].

The above results are for the case of two-dimensional crystallization and recrystallization, which are found in such technically relevant situations as solidification or annealing of thin films, plates and shells. Hesselbarth [22] has shown that, while computation-intensive, three-dimensional simulations using cellular automata yield results in agreement with the JMAK theory for both homogenous and site-saturated nucleation without particles. The present study focusing on the effect of a second phase could be extended to three dimensions as well, where the effect of particles, fibers, plates and interconnected

Table 2. Mean grain size $\bar{A}$, mean grain aspect ratio $\bar{R}$, normal deviate Z_A for normalized grain size distribution $A/\bar{A}$ and normal deviate Z_R for normalized grain ratio distribution $R/\bar{R}$ between the parametric distribution and the baseline distribution

		$\bar{A}$	$\bar{R}$	Z_A	Z_R
Baseline					
$a = 64, f = 0.125,$	$r = 4$	214.5 ± 1	1.355 ± 0.005	0.0533[a]	1.11[a]
$a = 64, r = 4,$	$f = 0$	225	1.28	0.240	6.50
	$f = 0.03125$	224	1.29	0.619	5.65
	$f = 0.0625$	222	1.34	0.126	1.15
	$f = 0.25$	198	1.47	0.337	5.21
$f = 0.125, r = 4,$	$a = 4$	211	1.30	0.222	4.46
	$a = 16$	210	1.31	0.448	4.31
	$a = 256$	220	1.46	0.155	9.22
$a = 64, f = 0.125,$	$r = 1$	219	1.35	0.0443	0.666
	$r = 16$	201	1.70	0.732	10.9
	$r = 64$	172	3.16	0.851	59.2

[a]Normal deviate between two separate simulations carried under baseline conditions.

skeletons on the kinetics of the matrix recrystallization could be explored.

5. CONCLUSIONS

The two-dimensional cellular automaton algorithm introduced by Hesselbarth and Göbel [21] for the recrystallization of single-phase materials is extended to the case of a matrix containing an inert, immobile second phase. The effect of second phase particles is assumed to be solely through geometric impingement upon contact with growing grains. Various particle sizes, area fractions and aspect ratios are investigated for conditions of continuous grain nucleation in the matrix.

Particles are found to influence the kinetics of recrystallization by lowering the Avrami exponent and increasing the time necessary for full recrystallization: within the parameters explored, the effect is largest for particles with high aspect ratios which prevent growth in the direction perpendicular to their long axis. Increasing particle area fraction has a similar but smaller influence, while the effect of particle size is very small. These effects are not predicted by a Johnson–Mehl–Avrami–Kolmogorov equation modified for the presence of inert particles, because the size and shape of the particles cannot be taken into account in the derivation.

Inert particles also influence both the mean size of recrystallized grains, which decreases with decreasing particle size and increasing particle aspect ratio and area fraction, and the mean aspect ratio of recrystallized grains, which increases with an increase of the above parameters. The normalized grain size distribution is however unaffected by the particles, unlike the normalized grain aspect ratio distribution which exhibits significant differences as particle parameters are varied.

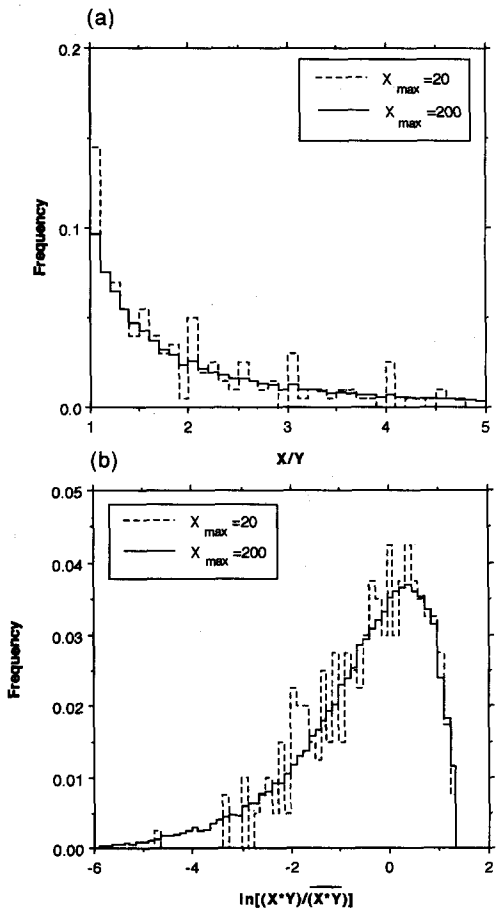

Fig. 12. (a) Frequency plots for all possible values of the ratio of integers x/y, where x and y are positive integers less than a maximum value $x_{max} = 20$ or $x_{max} = 200$. (b) Frequency plots for all possible values of the product of integers $x \cdot y$ (normalized by the mean product $\overline{x \cdot y}$), where x and y are positive integers less than a maximum value $x_{max} = 20$ or $x_{max} = 200$.

Acknowledgements—C.F.P. gratefully acknowledges the support of the MIT Undergraduate Research Opportunity Program, and access to the MIT Athena Computation System. D.C.D. acknowledges the support of AMAX in the form of an endowed chair, as well as helpful discussions with Professor J.C. Eberly of the University of Pennsylvania and Professor A. Mortensen of MIT.

REFERENCES

1. W. A. Johnson and R. F. Mehl, *Trans. Am. Inst. Min. Engrs* **135**, 416 (1939).
2. M. Avrami, *J. chem. Phys.* **7**, 1103 (1939).

3. M. Avrami, *J. chem. Phys.* **8,** 212 (1940).
4. A. E. Kolmogorov, *Akad Nauk SSSR, Izv. Ser. Mat.* **1,** 355 (1937).
5. K. Marthinsen, T. Furu, E. Nes and N. Ryum, *Simulation and Theory of Evolving Microstructures* (edited by M. P. Anderson and A. D. Rollett), p. 87. TMS, Warrendale, Pa (1990).
6. H. J. Frost and C. V. Thompson, *Acta metall.* **35,** 529 (1987).
7. C. W. Price, *Recrystallization '90* (edited by T. Chandra), p. 789. TMS, Warrendale, Pa (1990).
8. O. Ito and E. R. Fuller, *Acta metall. mater.* **41,** 191 (1993).
9. F. J. Humphreys, *Mater. Sci. Technol.* **8,** 135 (1992).
10. D. Juul Jensen, *Scripta metall. mater.* **27,** 1551 (1992).
11. K. W. Mahin, K. Hanson and J. W. Morris, *Acta metall.* **28,** 443 (1980).
12. K. Marthinsen, O. Lohne, and E. Nes, *Acta Metall.* **37,** 135 (1989).
13. T. O. Saetre, O. Hunderi and E. Nes, *Acta metall.* **34,** 981 (1986).
14. T. O. Saetre, O. Hunderi, E. Nes and N. Ryum, *Aluminum Alloys, their Physical and Mechanical Properties* (edited by E. A. Starke and T. H. Sanders), p. 1757. EMAS, West Midlands, England (1986).
15. T. Furu, K. Marthinsen and E. Nes, *Mater. Sci Technol.* **6,** 1093 (1990).
16. D. J. Srolovitz, G. S. Grest and M. P. Anderson, *Acta metall.* **34,** 1833 (1986).
17. D. J. Srolovitz, G. S. Grest, M. P. Anderson and A. D. Rollett, *Acta metall. mater.* **36,** 2115 (1988).
18. A. D. Rollett, D. J. Srolovitz, R. D. Doherty and M. P. Anderson, *Acta metall. mater.* **37,** 627 (1989).
19. A. D. Rollett, D. J. Srolovitz, R. D. Doherty, M. P. Anderson and G. S. Grest, *Simulation and Theory of Evolving Microstructures* (edited by M. P. Anderson and A. D. Rollett), p. 103. TMS, Warrendale, Pa (1990).
20. A. D. Rollett, M. J. Luton and D. J. Srolovitz, *Acta metall. mater.* **40,** 43 (1992).
21. H. W. Hesselbarth and I. R. Göbel, *Acta metall. mater.* **39,** 2135 (1991).
22. H. W. Hesselbarth, *Braunschweig Series on Mechanics*, Vol. 4-1992. TUB, Braunschweig, Germany (1992).
23. M. Rappaz and C. A. Gandin, *Acta metall. mater.* **41,** 345 (1993).
24. A. D. Rollett, D. J. Srolovitz, M. P. Anderson and R. D. Doherty, *Acta metall. mater.* **40,** 3475 (1992).
25. E. Nes, N. Ryum and O. Hunderi, *Acta metall.* **33,** 11 (1985).
26. T. Furu, K. Marthinsen, U. Tundal, N. Ryum and E. Nes, *Materials Architecture* (edited by J. B. Bilde-Sorensen), p. 343. Risø, Roskilde, Denmark (1989).
27. F. J. Humphreys, *Scripta metall. mater.* **27,** 1551 (1992).
28. O. Hunderi and N. Ryum, *Acta metall.* **29,** 1737 (1981).
29. D. J. Srolovitz, M. P. Anderson, P. S. Sahni and G. S. Grest, *Acta metall.* **32,** 793 (1984).
30. M. P. Anderson, G. S. Grest and D. J. Srolovitz, *Scripta Metall.* **19,** 225 (1985).
31. H. J. Frost, C. V. Thompson and D. T. Walton, *Acta metall. mater.* **38,** 1455 (1990).
32. V. Y. Novikov, E. A. Zalem and Y. A. Smirnova, *Acta metall. mater.* **40,** 3459 (1992).
33. G. N. Hassold, E. A. Holm and D. J. Srolovitz, *Scripta metall. mater.* **24,** 101 (1990).
34. E. A. Holm, G. N. Hassold and D. J. Srolovitz, *Simulation and Theory of Evolving Microstructures* (edited by M. P. Anderson and A. D. Rollett), p. 57. TMS, Warrendale, Pa (1990).
35. L. L. Lapin, *Probability and Statistics for Modern Engineering*. Brooks, Monterey, Calif. (1983).

APPENDIX 1

Non-Parametric Statistics

In order to compare the distributions of grain geometrical characteristics (normalized grain size and aspect ratio) for simulations carried under different particle geometric parameters, a non-parametric statistical test is used, which does not make any assumptions concerning the distribution of the populations considered. The Wilcoxon Rank-Sum Test [35] compares two populations 1 and 2 (e.g. populations of grains in matrices containing particles with different aspect ratios) constituted of a number of observations (e.g. normalized grain size) m_1 and m_2 respectively. The two populations are first merged into a single population for which each observation is ranked in ascending order. The ranked observations are then separated into their original populations, and the sum W of the observation ranks for population 1 is computed. Under the null hypothesis of identical populations (e.g. the two populations have the same normalized grain size distribution), there is an equal chance for any particular rank to belong to population 1 or 2. Assuming a normal sampling distribution for W, the normal deviate Z for the Wilcoxon Rank–Sum Test defined as

$$Z = \frac{W - \dfrac{m_1(m_1 + m_2 + 1)}{2}}{\sqrt{\dfrac{m_1 m_2 (m_1 + m_2 + 1)}{12}}}$$

can be compared to tabulated critical values Z_c for a given significance level [35].

APPENDIX 2

JMAK Derivation for a Matrix Containing Inert Particles

In the original JMAK derivation, the extended volume fraction of recrystallized matrix x_e, corresponding to the volume fraction recrystallized at time t if the overlap of grains is neglected, is

$$x_e = kt^n \tag{A1}$$

where k is a function of the growth rate, nucleation rate and geometry of the growing grains, and the Avrami exponent n varies between 1 and 4, depending on the dimensionality of growth and the time dependence of the nucleation rate.

Assuming a random distribution of grains and assuming that the ratio of increase in actual volume fraction of recrystallized matrix dx to increase in extended recrystallized volume fraction dx_e, is equal to the unrecrystallized volume fraction $1 - x$

$$\frac{dx}{dx_e} = 1 - x \tag{A2}$$

the classical JMAK equation is obtained by combining equations (A1) and (A2), integrating and rearranging

$$x = 1 - \exp(-kt^n). \quad \text{(A3)}$$

We now derive the case of a composite containing inert, non-recrystallizing particles of volume fraction f and a recrystallizing matrix of volume fraction $(1-f)$. We make the same assumption as above, but take into account that a fraction f of the composite is occupied by particles which do not recrystallize

$$\frac{dx}{dx_e} = 1 - x - f. \quad \text{(A4)}$$

Separation of variables, and integration of equation (A4) between 0 and x_e, and 0 and x, respectively, with a change of variable $z = 1 - f - x$, yields after rearrangement and use of equation (A1):

$$x = (1-f)[1 - \exp(-kt^n)]. \quad \text{(A5)}$$

The volume fraction of recrystallized composite varies between $x = 0$ and $x = 1 - f$, and, as expected, equation (A5) simplifies to equation (A3) for $f = 0$. If, instead of considering the total composite volume as the sum of volumes of particles and matrix, the total volume is defined as that of the matrix only, the volume fraction recrystallized composite normalized by the matrix volume fraction $x' = x/(1-f)$ varies between 0 and 1 and equation (A5) is equivalent to equation (A3). We thus conclude that, assuming that particles reduce the extended volume according to equation (A4), particles have no impingement effect on the kinetics of recrystallization of the *matrix*.

The above result is not immediately intuitive since impediment between a growing grain and a non-growing particle would be expected to vary differently with time than the impingement between two growing grains. A purely geometric approach to the above solution is sketched in Figs A1–A4. Figure A1 shows the extended recrystallized volume, actual recrystallized volume and total volume used in the original JMAK derivation [equations (A1)–(A3)]. Figure A2 corresponds to the situation where a fraction of the total volume is occupied by particles. The exact location of the particles does not influence the amount of extended volume overlapping with particles, since grain nucleation occurs randomly within the available volume and impingement is isotropic. The particles can thus be gathered together, as in Fig. A3, which is equivalent to Fig. A4, which itself is equivalent to Fig. A1, albeit with a smaller total volume. It can thus be concluded that the particles do not alter the recrystallization kinetics of the matrix. It also follows that the shape and size of the particles have no influence on the recrystallization, as only the volume of the particle is considered in the derivation.

However, if it is assumed that particles have an effect on the nucleation rate (by particle stimulated nucleation) or growth (Zener pinning), equation (A5) must be modified and the particles are predicted to alter the overall kinetics of recrystallization.

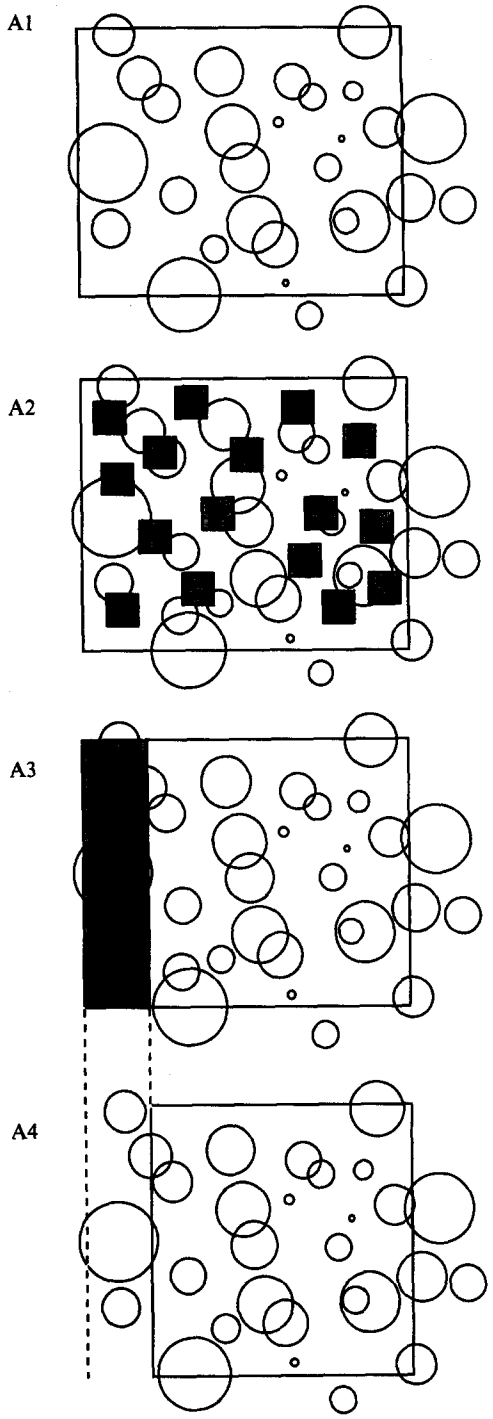

Fig. A1. Impinging spherical grains in a total volume (given by the box): the extended volume is the sum of the volumes of the grains within the total volume, the recrystallized volume is the extended volume minus the volume of overlapping grains.

Fig. A2. Part of the total volume in Fig. A1 is occupied by shaded cubic particles.

Fig. A3. Same volume as Fig. A2, with particles rearranged.

Fig. A4. Same volume as Fig. A3, considering only the matrix volume. This situation is equivalent to Fig. A1, with a smaller total volume.